JTTEE5 5:445-456

Rapid Solidification and Microstructure Development during Plasma Spray Deposition

S. Sampath and H. Herman

Plasma spray processing is a well-established method for forming protective coatings and free-standing shapes from a wide range of alloys and ceramics. The process is complex, involving rapid melting and high-velocity impact deposition of powder particles. Due to the rapid solidification nature of the process, deposit evolution also is complex, commonly leading to ultrafine-grained and metastable microstructures. The properties of a plasma-sprayed deposit are directly related to this complex microstructure. This paper examines the solidification dynamics and the resultant microstructures in an effort to establish a processing/microstructure relationship. Existing models in the literature developed for splat cooling have been extended and applied for examining the rapid solidification process during plasma spraying. Microstructural features of the splats that are produced by individual impinging droplets are examined through scanning and transmission electron microscopy. The relation of dimensions and morphologies of these individual splats to the consolidated deposit microstructure is considered. In addition, the distinguishing features in the solidification and microstructural development between air plasma spraying and vacuum plasma spraying are explored, and a unified model is proposed for splat solidification and evolution of the microstructure.

Keywords electron microscopy, metastable phases, microstructure development, rapid solidification, texture

1. Introduction

PLASMA spraying has been used extensively for more than three decades to apply protective coatings on a variety of substrates. The process is an elevated-temperature, higher-velocity version of the more generic material processing technique of thermal spraying, in which material is melted in a hot flame and the melt is accelerated toward a substrate, where it rapidly solidifies. It is a versatile technique and has been used to produce metallic, ceramic, cermet, and composite coatings for such diverse applications as corrosion protection, wear resistance, thermal barriers, high-temperature oxidation protection, and reclamation work. More recently, plasma spray forming methods have been used to produce near-net shapes of high-temperature alloys, intermetallics, ceramics, and composite materials (Ref 1).

Rapid impact deposition of plasma-melted particles of a wide range of alloys and ceramics can yield highly metastable structures in both films and freestanding forms. Plasma spray processing, which combines the steps of melting, quenching, and consolidation into a single operation, can be considered an upscaled version of droplet deposition from the melt. Conventional air plasma spraying (APS) has long been considered to be an effective rapid solidification processing (RSP) technique, since it allows continuous quenching while permitting material buildup. The process can be referred to as continuous metastable materials forming (Ref 2). The RSP effects of plasma spraying were observed by Moss (Ref 3) in the form of high supersaturation of vanadium in aluminum. Krishnananda and Cahn (Ref 4) observed significant solute supersaturation in APS-formed Al-6Cu alloys. Giessen et al. (Ref 5) have produced amorphous zirconium-copper by plasma spraying onto a rapidly rotating disk within an inert gas chamber. A number of investigators have tried to form amorphous alloy protective coatings using plasma spray (Ref 6-8).

Although APS deposition yields rapid solidification, defects such as porosity, oxide inclusions, residual stresses, and unmelted particles result. With the advent of vacuum plasma spraying (VPS), it is possible to produce well-adhered, dense metallic alloy deposits with minimal oxidation. This process has been used principally by the gas turbine industry for the production of oxidation-resistant alloy coatings (NiCoCrAlY) on turbine blades. Because of its unique characteristics, VPS is being considered for the production of wear- and corrosion-resistant coatings (Ref 9, 10).

The VPS-formed deposit is maintained at much higher temperatures than is the APS deposit due to the increased interaction between the plasma jet and the substrate (caused by the longer plasma flame), coupled with the absence of convective cooling of the substrate.* This high temperature (800 to 1000 °C) of the substrate causes self-annealing of the deposit, thereby considerably altering the rapidly solidified structure. It has been shown that this self-annealing can be beneficial, since it provides stress relief and recrystallization and results in enhanced interparticle bonding (Ref 11). The reduction of residual stresses permits buildup of thick deposits, and thus VPS can become an effective means for consolidating powders and composites for the production of freestanding forms for high-performance applications (Ref 12, 13).

Researchers at General Electric have examined a number of nickel-base alloys using VPS (Ref 14-18). Their results indicate that the rapid solidification of the molten droplets occurs during deposition in a low-pressure environment, with the deposits achieving nearly theoretical density. They further reported that

S. Sampath and **H. Herman,** Thermal Spray Laboratory, Department of Materials Science and Engineering, State University of New York, Stony Brook, NY 11794-2275, USA.

*Vacuum plasma spraying is actually a reduced-pressure, inert gas chamber process, operating at about 60 mbar. It is also referred to as low-pressure plasma spraying (LPPS).

even in the case of substrates heated to 900 °C prior to plasma deposition, the quench rates were likely equivalent to that of RSP melt-spun ribbons (i.e., $>10^6$ K/s) (Ref 18).

Several studies have been reported on plasma flame diagnostics and particle melting efficiency for both APS and VPS (Ref 19, 20). Houben (Ref 21) has described in considerable detail the physical considerations of splat formation through heat transfer and mechanical models. He has identified the various types of splat morphologies, described broadly as "pancake type" and "flower type." He has further shown that splat morphology is affected by the velocity of the impinging droplet; increased velocity causes enhanced flattening and spreading of the droplet. More recently, Dykhuizen (Ref 22) has critically reviewed the impact, spreading, and solidification of thermal spray droplets, addressing the role of droplet splashing, substrate temperature, surface tension, and contact resistance. Vardelle et al. (Ref 23) have related particle parameters (velocity, size, and temperature) to flattening and cooling processes and have shown that contact resistance is the key factor for cooling of impact droplets. It was further demonstrated that contact resistance is affected by substrate condition (roughness, presence of oxides) and substrate temperature. Lower oxide content on the surface and higher temperature resulted in more uniform spreading of the droplet. Moreau et al. (Ref 24) have examined substrate roughness effects on flattening and cooling times. They reported that flattening times were significantly reduced for rough surfaces compared to smooth surfaces. Roughened surfaces showed greater fragmentation of the particle, which may account for the phenomenon.

Many of these investigations provide limited information on the solidification dynamics and the related microstructures of the deposits. The purpose of the present study was to examine the metallurgical aspects of splat formation and solidification. This differs from the previously mentioned studies in that solidification and crystal growth of the flattened droplet are examined within the context of crystal nucleation and growth of the solidification front and the subsequent microstructure development. Studies of flattening and spreading and the present investigation on solidification and microstructure development are not mutually exclusive; therefore, interrelationships among these parameters have been examined to a degree.

This paper examines correlations between solidification processes and microstructures for APS and VPS processes. The distinguishing features between the two processes are also examined and correlated with microstructure. Nickel-base alloys are studied due to their wide use in plasma spraying. The metallurgical changes occurring in these systems during the steps of high-velocity impact deposition, rapid solidification, and rapid thermal annealing associated with VPS enable improved understanding of the nature of the process. Although the present study has primarily used aluminum and nickel for the analysis, the basic phenomena are generally applicable to other metallic, intermetallic, and ceramic systems. It is anticipated that such analyses will lead to control of the deposit microstructure and, consequently, of material properties.

Table 1 Material specifications and powder characteristics

Powder	Composition, wt %	Characteristics
Nickel	Ni	Precipitated
Aluminum	Al	Gas atomized
Ni-Al alloy	Ni-5Al	Gas atomized
Ni-Cr alloy	Ni-50Cr	Gas atomized
Molybdenum	Mo	Spray densified

2. Experimental Method

This study used standard commercial feedstock powders (Table 1). All of the powders were plasma sprayed using both APS and VPS processes. Plasma spraying was carried out in a Plasma-Technik automated APS/VPS system. Table 2 lists the typical spray parameters employed. Variations of these parameters were used to produce fully melted, dense, homogeneous deposits of the various powders. Substrate temperature measurements were performed by mechanically inserting a thin chromel-alumel thermocouple into a hole drilled into the back of the substrate and positioned approximately 1 mm from the outer surface. The temperatures were recorded continuously with a millivolt chart recorder.

Two types of specimens were formed for the transmission electron microscope (TEM) study. Individual flattened particles (splats) were produced by rapidly traversing the gun (100 mm/s) across a polished copper substrate at low powder feed rates (<0.25 kg/h), thus enabling electron transparent regions to be directly observable in the TEM. Cross sections and lateral sections of deposits for TEM were produced from bulk deposits sprayed to a thickness of 0.4 to 0.6 mm, which were ground and polished to 0.05 mm thickness and ion beam milled to produce an electron transparent thickness. X-ray diffractometry was performed on both the front and back sides of freestanding deposits, which were removed after spraying onto steel substrates. Copper Kα radiation was used as the x-ray source.

3. Results and Discussion

Plasma-sprayed deposits are composed of cohesively bonded splats created by the high-rate impact and rapid solidification of a high flux (millions of particles/cm^2/s) of plasma-melted particles, which result in "brick wall"-type microstructures entwined in complex arrays (Ref 25). The physical properties and behavior of such a deposit are expected to depend on the cohesive strengths among the splats, the size and mor-

Table 2 Plasma spray parameters

Variable	APS	VPS
Gun	PT-F4-HB/MB(a)	PT-F4V(a)
Current, A	500	650
Voltage, V	68	68
Primary gas (argon), slpm	50.4	50
Secondary gas (H_2), slpm	8.0	9
Powder carrier (argon), slpm	3.5	2
Feed rate, g/min	50	50
Chamber pressure	1 bar (atm)	60 mbar
Spray distance, mm	110	300

(a) PT, Sulzer Plasma Technik

phology of the porosity, the occurrence of cracks and defects, and, finally, on the microstructure within the splats themselves.

The microstructures of plasma-sprayed deposits are ultimately based on the solidification of many individual molten droplets. A splat results when a droplet of molten material, tens of micrometers in diameter, melted in the plasma flame, strikes a surface at high velocity, flattens out, and solidifies. The collection of these splats forms the deposit. The dynamics of deposit evolution during plasma spraying involve many factors. The mechanistic or physical aspects of splat formation deal with the spreading of the molten droplet, interactions with the substrate, and so forth. These characteristics are affected by the temperature of the splat, splat viscosity, and surface tension. Splat morphology depends on a variety of factors, the most important of which are particle velocity, temperature, diameter, and substrate surface profile. Further considerations involve the metallurgical behavior of the splat, which deals with the cooling rate, solidification criteria, nucleation and growth of crystals, and phase formation. These aspects of splat formation and solidification are complex and interrelated. This study primarily examines the metallurgical aspects of deposit formation.

The cooling and solidification rates for a plasma-sprayed deposit depend on the solidification of individual splats and substrate conditions. It has been suggested that cooling rates achieved in APS are on the order of 10^7 deg/s (Ref 3, 26). Moreau et al. (Ref 27, 28) have used two color pyrometric techniques to directly measure temperature profiles and cooling curves for solidifying molybdenum and niobium particles during plasma spray deposition. They reported cooling rates on the order of 10^8 K/s for solidification on conducting substrates. In the present study, an experimental examination of the cooling rate has been performed and examined analytically with reference to appropriate models for aluminum and nickel, and its influence on microstructure development explored.

3.1 *Solidification Parameters*

Plasma spraying involves rapid conduction cooling of 10 to 100 μm droplets onto a thermally conductive substrate. Subsequent to the deposition of the initial layers, solidification of the molten droplets occurs on prior deposited material. The mode of heat transfer for the splat is thought to be rapid conduction cooling through the substrate or prior deposited splats. In effect, this process is similar to splat quenching by the Duwez gun technique (Ref 29), except for differences in size of the droplet, velocity of the impinging particles, and nonnormal spreading of the droplet. Thus, various established models of splat quenching are applicable here. A number of considerations relative to splat quenching have been applied to this case. The average cooling rates were estimated from indirect and direct means. The indirect techniques involved cooling rate measurements, using correlations to features of rapid solidification, such as secondary dendrite arm spacing and splat thickness. In addition, results are included from direct cooling rate measurements, which were obtained from an earlier study through substrate temperature measurements (Ref 30) and those reported in the literature obtained from optical pyrometric methods (Ref 27).

Three solidification front morphologies are possible under low to moderate cooling rates. This is illustrated in Fig. 1(a) (Ref 31), where the front morphology is controlled by the temperature gradient in the liquid (G_l) and the interface velocity (R). The slope of G_l/R determines the stability of the plane-controlling variable—namely, the temperature gradient or solute gradient. The dominance of the temperature gradient stabilizes the plane front, while the solute gradient leads to segregated microstructures (cellular or dendritic). In the case of high cooling rates such as those experienced in RSP, Fig. 1(a) is modified as shown in

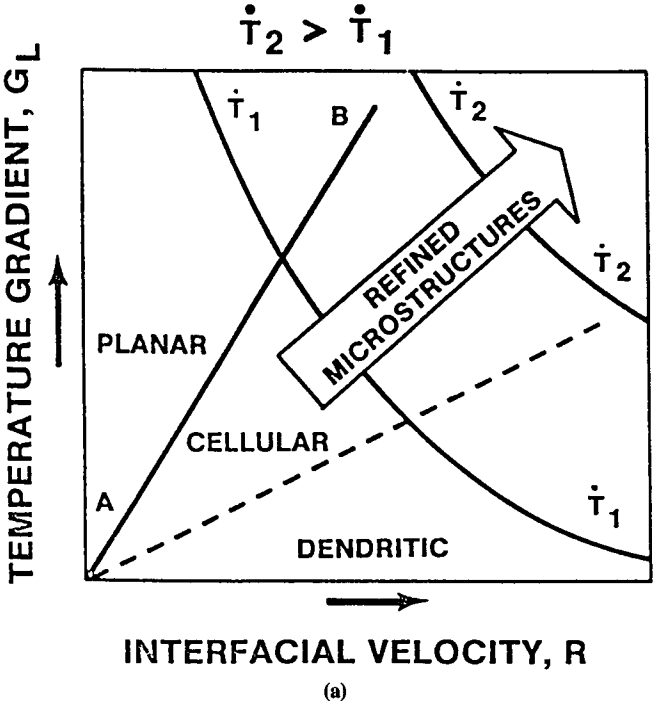

(a)

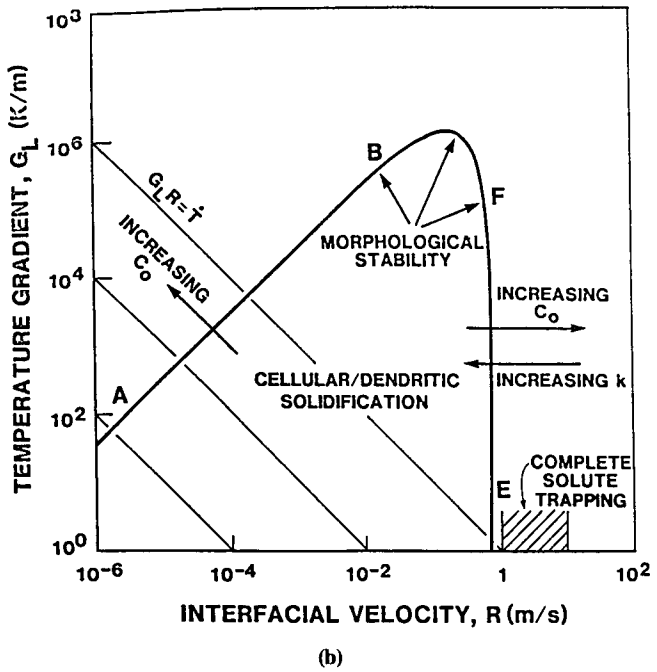

(b)

Fig. 1 Relationship between liquid temperature gradient and solidification rate describing the morphology of the solidification front under low to moderate (a) and rapid solidification (b) conditions. T_1 and T_2 are cooling rates, and average cooling rate $T = G_l R$. Source: Ref 31

Table 3 Relationship of splat thickness to cooling rate

Splat thickness, μm	Cooling rate (nickel-base alloys), deg/s (Eq 2b)	Cooling rate (aluminum alloys), deg/s (Ref 26)
1	3.2×10^{8}	5.8×10^{7}
5	6.4×10^{7}	1.2×10^{7}
10	3.2×10^{7}	5.8×10^{6}

Fig. 1(b), where the morphological instability is capped off (segment B-F); when solidification front velocities are sufficiently large, morphological stability is reestablished and plane front growth ensues. These attributes and regimes of applicabilities are described in detail in Ref 31. The interfacial velocity for morphological stability is material dependent and is available in the literature for several systems (Ref 31).

3.2 *Cooling Rates*

3.2.1 Dendrite Arm Spacing Correlation

The relationship of dendrite arm spacing to cooling rate follows the equation

$$d = a\,(Q_{avg})^{-n} \qquad \text{(Eq 1)}$$

where d is secondary dendrite arm spacing (in microns), Q_{avg} is average cooling rate (K/s), and a and n are material-dependent constants (Ref 32, 33). For nickel-base alloys, the constants a and n are thought to be valid for all cooling rates (Ref 28):

$$a = 33.85$$

$$n = 0.4$$

The secondary dendrite arm spacing was obtained from TEM of a nickel splat to be 25 nm (Ref 30). The corresponding cooling rate for this spacing as obtained from Eq 1 is 6.7×10^{7} K/s, which is similar to that reported for plasma-sprayed aluminum-silicon alloys by Wilms (Ref 26) using dendrite arm spacing correlation and by Murakami et al. (Ref 34) for iron-carbon-silicon alloys.

3.2.2 Splat Thickness Correlation

A relationship is expected between cooling rate and splat thickness during liquid quenching (Ref 35). Huang et al. (Ref 36) have reported such a relationship for nickel-base superalloys obtained by melt spinning:

$$s = 2.7\times t^{1/2} \qquad \text{(Eq 2a)}$$

where s is the ribbon (or splat, in this case) thickness in microns, and t is the solidification time. The cooling rate Q (K/s) is:

$$Q = 320\times s^{-2} \qquad \text{(Eq 2b)}$$

It is worthwhile to note that although Eq 2(a) and (b) resemble solidification equations under ideal cooling conditions, they have been used to depict the empirical dependence of splat thickness to cooling rate.

A typical plasma spray splat varies from 1 to 10 μm in thickness. For these conditions, a direct application of Eq 2(b) yields a cooling rate on the order of 10^{7} K/s. Using theoretical considerations, similar results were obtained by Wilms (Ref 26) for plasma-sprayed aluminum-silicon alloys. Cooling rate variations with splat thickness are given in Table 3, which includes the results obtained in this study as well as those reported in Ref 26.

3.2.3 Direct Cooling Rate Measurements

Predecki et al. (Ref 37) obtained cooling rates directly by splat cooling aluminum on nickel/silver substrate couples. Subsequently, similar measurements were reported by Harbur et al. (Ref 38). It has been suggested that these measurement techniques are inaccurate due to uncertain effects of response time lag, arising from imperfect contact between melt and thermocouple, and to the effects of material overlapping at different stages of cooling (Ref 39). Despite these uncertainties, this technique yields valuable information on the orders of magnitude for the cooling rates. The cooling rates obtained by monitoring the change in substrate temperature are presented here. The procedure and the results have been reported elsewhere (Ref 30), and the results are summarized in Table 4. Moreau et al. (Ref 27) obtained cooling rates, apparent duration of the flattening process, and the cooling speed for solidifying molybdenum splats using rapid two-color pyrometric methods. The thermal radiation emitted by the solidifying particle was monitored by shielding the plasma flame away from the particle.

The cooling rates estimated from the various techniques are also summarized in Table 4. All three techniques indicate an average cooling rate of 10^{7} to 10^{8} K/s for splat solidification during plasma spraying. These high cooling rates confirm that plasma spraying yields rapid solidification.

Variations in cooling rates can arise due to differences in substrate thermal conductivity. Moreau et al. (Ref 28) have studied this effect during plasma spraying of molybdenum powder on copper, ZrO_2, and glass substrates. The deposition on ZrO_2 and glass substrates showed an order of magnitude lower cooling rate as compared to copper substrates. Even so, the cooling rates were greater than 10^{7} K/s (i.e., in the regime of RSP).

3.3 *Solidification Rates, Heat-Transfer Coefficient, and Degree of Constitutional Supercooling*

The solidification parameters directly related to structure, such as solidification rate, heat-transfer coefficient, and type of cooling, were derived from cooling rate measurements. The relationship between cooling rate and heat-transfer coefficient for Newtonian cooling conditions can be expressed as (Ref 37):

$$Q = \frac{h(T_t - T_S)}{\rho C_p s} \qquad \text{(Eq 3)}$$

where Q (equal to dtp/dt) is the cooling rate (K/s), h is the heat-transfer coefficient (W/m^2 · K), T_S is the substrate temperature (K), ρ is the density of the splat (kg/m^3), T_t is the melting point of the splat (K), C_p is the specific heat capacity of the splat (J/kg · K), and s is splat thickness (m).

Table 4 Average cooling rates obtained from various techniques

Technique	Nickel and nickel alloys, K/s	Aluminum and aluminum alloys, K/s	Molybdenum, K/s
Dendrite arm spacing	6.7×10^7	9×10^6(a)	...
Splat thickness correlation (5 μm)	6.4×10^7	1.2×10^7(a)	...
Direct cooling rate measurement	6.8×10^7(b)	2×10^8(b)	2×10^8(c)

(a) Ref 26. (b) Ref 30. (c) Ref 27

Table 5 Solidification variables derived from cooling rates

Material	Average cooling rate, K/s	Heat-transfer coefficient, W/m²	Nusselt's number (hd/k_s, d = 5 mm)	Solidification rate (R)(a), cm/s	G_l/R, K·s/cm²
Nickel	7×10^7	1.4×10^6	0.069	46	2.2×10^4
Aluminum	1.5×10^8	3.5×10^6	0.005	15	3.7×10^4
Molybdenum	2×10^8	1.8×10^6	0.063	150	1.2×10^4

(a) Assuming no isothermal delay

The type of cooling (defined as ideal, Newtonian, or intermediate*) can be obtained from estimation of Nusselt's number (hd/k_s) (Ref 35). The values obtained from the previous equations are listed in Table 5 and indicate the type of cooling to be "intermediate," bordering on "Newtonian." This suggests that the cooling rates are predominantly interface controlled and are in agreement with Ruhl's model for splat cooling (Ref 35).

The solidification rate, assuming no isothermal delay, can be obtained using this relationship (Ref 39):

$$R = \frac{h(T_t - T_S)}{\rho L_F} \quad \text{(Eq 4)}$$

where R is the solidification rate (m/s), and L_F is the latent heat of fusion of the particle (J). Equation 4 is applicable for Newtonian cooling conditions.

The solidification velocities compare well with those predicted by Shingu and Ozaki (Ref 40) for splat cooling, using heat-transfer calculations and molecular kinetic considerations. The degree of constitutional supercooling provided by the characteristic ratio G_l/R (Ref 41) has been calculated for the solidification of a single splat during plasma spray deposition. G_l is the thermal gradient in the liquid, given by:

$$G_l = \frac{T_t - T_{sl}}{s} \quad \text{(Eq 5)}$$

where T_t is the melting point of the splat material (K); T_{sl} is the temperature of the solid/liquid interface, which in this case can be represented as the undercooled solidification temperature (K); and s is average splat thickness (μm).

**Ideal cooling* applies if no discontinuity exists at the interface and if there is a relatively large thermal gradient in both the splat and the substrate. *Newtonian cooling* is applicable for small values of heat-transfer coefficients and where the heat transfer is completely interface controlled. Such a condition would exist if there were very small or no thermal gradients in the splat and the substrate. *Intermediate cooling* applies to a regime of cooling between the two.

For an average splat thickness of 5 μm and an undercooling of 0.3 T_m (Ref 33), the G_l value is 10^6 K/cm for nickel and 5.6×10^5 K/cm for aluminum. The corresponding G_l/R values are listed in Table 5. (The typical value of 0.3 T_m for undercooling is based on the maximum achievable undercooling for homogeneous nucleation.)

The large values of G_l/R represent a regime close to absolute stability in the solidification front. Cheeks et al. (Ref 17) have calculated G_l/R values of 5×10^5 K · s/cm² for LPPS of nickel-base alloys and have concluded that the criteria for absolute stability are satisfied and thus that planar growth occurs. (They assumed a growth rate of 0.1 cm/s.) Cohen and Mehrabian (Ref 41) indicated that for an Al-0.1Si alloy, the plane front is morphologically stable at $R > 100$ cm/s or at a G_l value greater than 10^4 K/cm. Based on these observations and the solidification parameters listed in Table 5, it is apparent that morphological stability with stable planar front is a likely mode of solidification in the core region of the splat during plasma spray deposition.

3.4 *Effect of Variables on Cooling Rate*

A number of variables affect cooling rates during plasma spraying. These include substrate surface morphology (i.e., roughness), substrate thermal properties, substrate temperature, and varying thickness regions within the splat. The type of cooling (ideal or Newtonian) depends on the splat thickness and can vary greatly within a given splat depending on the thickness at a given position within the splat. Since the cooling is predominantly interface controlled, the initial formation of a strong adhesive bond is essential for effective heat transfer between the splat and the substrate. Thus, the presence of entrapped air and surface oxides (for sprayed metals), which are common features in the APS deposit, can significantly reduce the heat-transfer coefficient and thus the cooling rates. Cooling rates can also vary greatly depending on the type of interface. For instance, for the first layers of deposit, the heat transfer is controlled by the thermal resistance of the splat/substrate interface; for subsequent layers, it is controlled by the thermal resistance of the splat/splat

interface, which can vary greatly for the range of substrate and coating materials. Moreau et al. (Ref 28) have shown that for many metals the splat/splat thermal resistance is lower than that of splat/substrate thermal resistance, even if the thermal conductivity of the substrate is higher than that of the deposited material.

In VPS, the problems associated with entrapped air and oxide stringers are largely absent; therefore, for a single layer of deposit, a very high cooling rate is expected. However, no convective cooling of the substrate is generally employed, and thus the temperature rise is substantial (up to 1000 °C) during continuous spraying, which leads to cooling rates that are smaller than APS by two orders of magnitude (see Table 4). This is illustrated in Fig. 2, representing the decrease in cooling rate with substrate temperature (Ref 30). These results are consistent with those predicted by Ruhl (Ref 35) for splat cooling. Although the cooling rates are still in the range for rapid solidification, prolonged exposure (several minutes to tens of minutes) of the deposit to these high temperatures causes self-annealing, leading to transformations of the rapidly solidified structure. This will be discussed further in this paper.

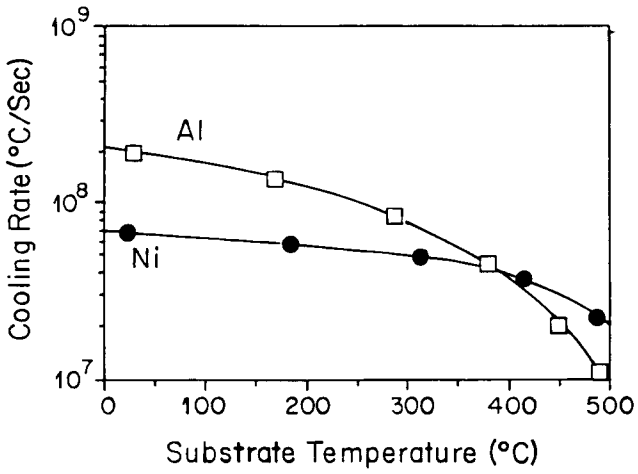

Fig. 2 Variation in cooling rate with substrate temperature during plasma spraying

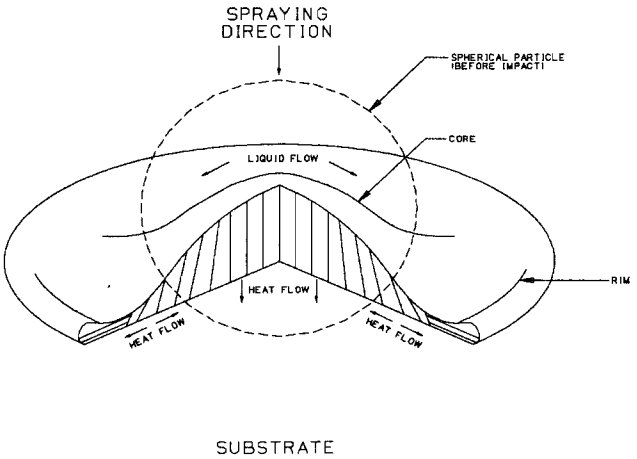

Fig. 3 Heat flow and related grain structure in a solidifying splat

4. Microstructure Development

4.1 *Splat Microstructures*

The evolution of the overall microstructure of plasma-sprayed deposits, of course, will be based largely on the solidification of individual splats as well as on the nature of the buildup of these splats into a deposit. The first model for the formation and solidification of a single plasma-sprayed splat produced by APS (Fig. 3) was originally proposed by Safai and Herman (Ref 42), but has been modified in this paper. Specifically, the modification lies in the nature of the grains within the splat. The earlier model showed a "brick wall"-type grain structure for the core region of the splat, whereas Fig. 3 shows an essentially columnar grain structure. This will be discussed more extensively later. It is suggested here that the present model is extendable to VPS. However, the melt-flow characteristics of the splat can vary from one material to another, depending on the melting point, degree of superheat, viscosity, and interactions with the substrate.

Figure 4 compares typical scanning electron microscope (SEM) micrographs of nickel splats on copper substrates produced by APS and VPS. The micrographs illustrate the enhanced flow behavior and better spreading of a VPS splat, attributed to higher particle velocity and temperature and the absence of surface oxidation. The APS splat, on the other hand,

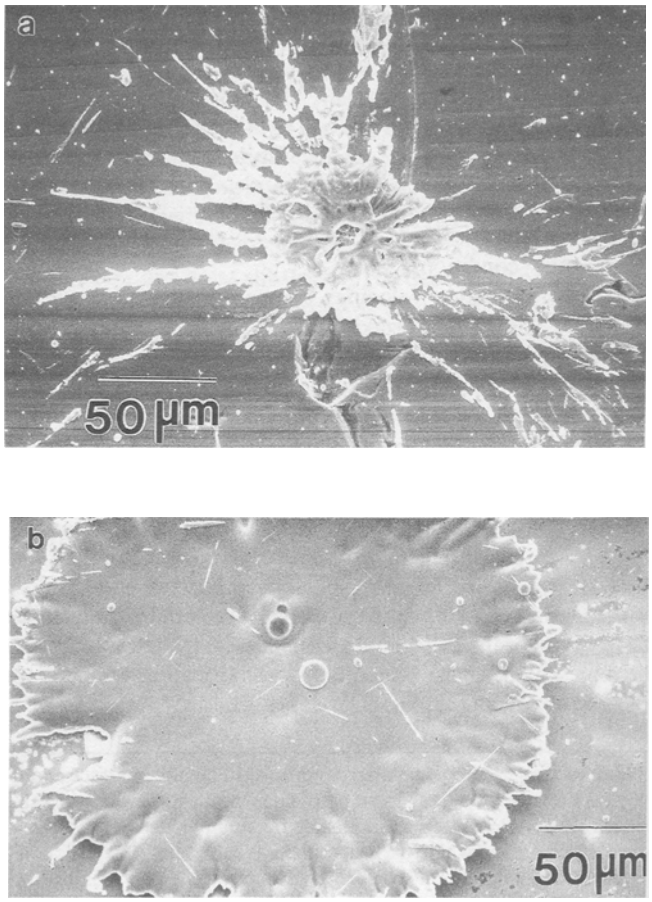

Fig. 4 SEM micrographs of a nickel splat. (a) APS (b) VPS

shows an arrested outward flow of the material. This reduced flow behavior of the APS splat can be attributed to increased splat viscosity due to oxidation. The presence of oxides may increase the splat/substrate interfacial friction, which may lead to an arrested flow of the solidifying droplet. During VPS processing the substrate temperature typically is higher, which can lead to improved spreading of the splat as indicated by Vardelle et al. (Ref 23). It is unlikely that this is the explanation in the present study, because the VPS splats were produced by rapid raster of the gun with minimal change in the substrate temperature.

Figure 5 compares TEM micrographs from the thin, electron transparent regions of the APS and VPS nickel splats. Figure 5(a) shows an APS nickel splat with a dendritic, fine-grained microstructure along its periphery, illustrating the arrested outward flow of molten material. The corresponding micrograph of a VPS splat in Fig. 5(b) reveals an elongated grain structure along the edge, illustrating greater outward flow behavior of the splat as compared with APS. These results are consistent with the SEM images shown in Fig. 4.

It is noted that the central core region represents most of the volume of the splat (Fig. 3). Hence, the microstructure and phase characteristics of the deposit are expected to be principally governed by the core region. The columnar microstructure suggested by Safai and Herman (Ref 42) has been verified here by TEM. Figure 6(a) is a cross-sectional TEM micrograph of an APS nickel coating on a steel substrate. The micrograph was taken from a region close to the interface, with the grains emanating from the interfacial region (substrate). Unlike the "brick wall" structure suggested earlier by Safai and Herman (Ref 42), the columns extend all the way across the splat cross section, consistent with Fig. 3. In VPS, instead of a columnar grain structure, a columnar cellular structure is observed (Fig. 6b), and this comes closer to resembling the "brick wall" structure. The diffuse cell walls are dislocation networks produced by alignment of edge dislocations along the wall. This effect is a product of polygonization in the material, which is a precursor to recrystallization. The formation mechanism of this microstructure has been described elsewhere (Ref 43). The cells observed in Fig. 6(b) have similar orientations, suggesting that the recrystallization process was incomplete.

4.2 *Texture*

The solidification rates listed in Table 5 indicate velocities of 10 to 50 cm/s for the solidification front. Under such conditions, it is expected that the fastest crystal growth direction will prevail. X-ray diffraction results (Table 6) from the back sides of both the APS and the VPS deposits, sprayed onto polished steel substrates, indicate a strong <200> texture in the deposit. This is expected, since <100> is the fastest growth direction for cubic materials (Ref 44). Such texture was also observed for Ni-5Al material, although to a lesser extent (Table 6). Moreau et al. (Ref 28) have also observed solidification texture in plasma-sprayed molybdenum on copper substrates. They observed increased intensities for the <200> reflections on the substrate side when sprayed onto a polished substrate. They also reported a strong texture on the front side of the coating, which was attributed to an increase in cooling rates due to better thermal contact resistance; however, this result has not been confirmed in this investigation.

These results suggest preferred, columnar-oriented growth within the core region of the splat. Such a microstructure is produced by heterogeneous nucleation of the solid at the interface, followed by growth of the solidification front perpendicular to the interface. The columnar microstructure in the core region of the splat is consistent with the measured solidification parameters, indicating morphological stability of the plane front. In reality, the coating is produced by the raining down of the molten particles onto the microscopically tortuous shape of the roughened (grit-blasted) surface, with the individual splats locked onto the surface irregularities (Ref 25).

Although each individual splat may have a texture associated with it, the accumulation of many of these <200> oriented splats develop randomly as a deposit, resulting in the annihilation of most of the preferred orientation. Safai and Herman (Ref 2, 42) reported random orientation of the grains in the middle and upper layers of an APS aluminum coating, which were proposed to arise due to a reduction in the cooling rate. Although this could be an important consideration in low melting alloys such as aluminum, no appreciable drop in cooling rates generally is expected due to small increases in substrate temperatures in APS (Ref 39). The presence of oxide layers on the surface of the de-

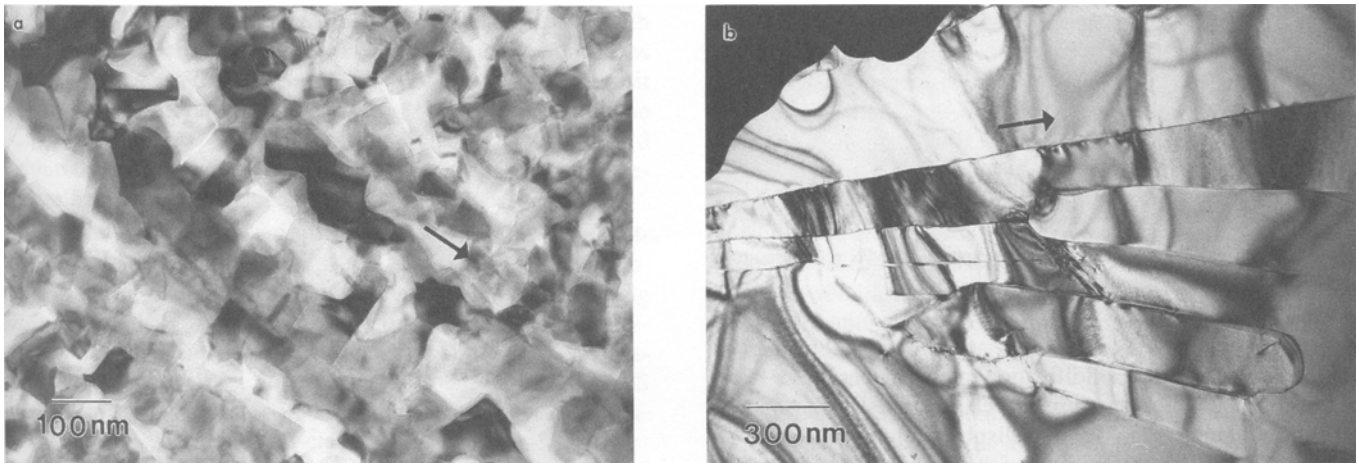

Fig. 5 TEM micrographs of thin, electron transparent regions within a nickel splat. Arrows indicate the direction of spreading along the splat periphery. (a) APS. (b) VPS

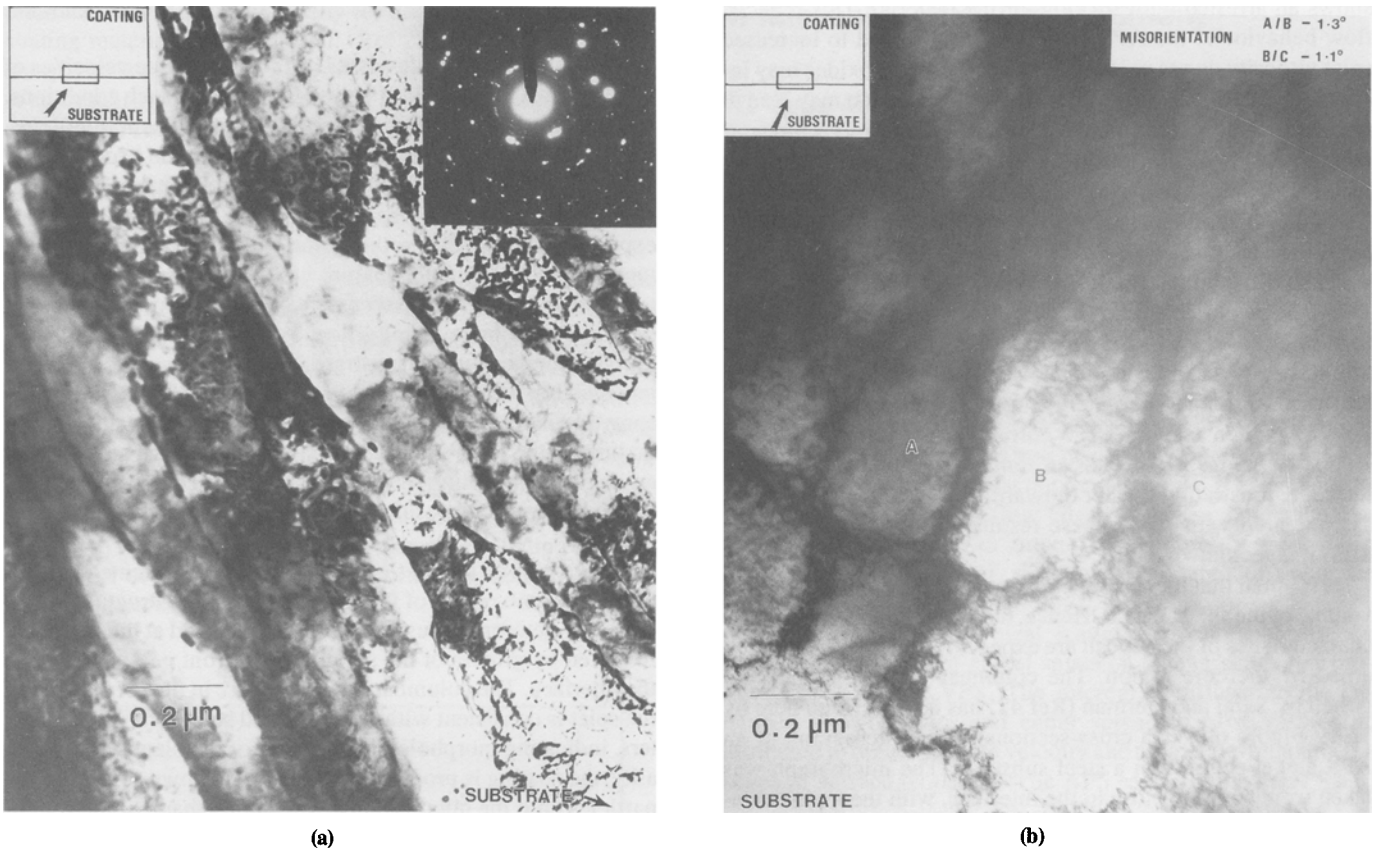

Fig. 6 TEM micrographs from cross section of a nickel deposit, taken within the deposit region. (a) APS. (b) VPS. The small misorientation between the cells in VPS is indicated

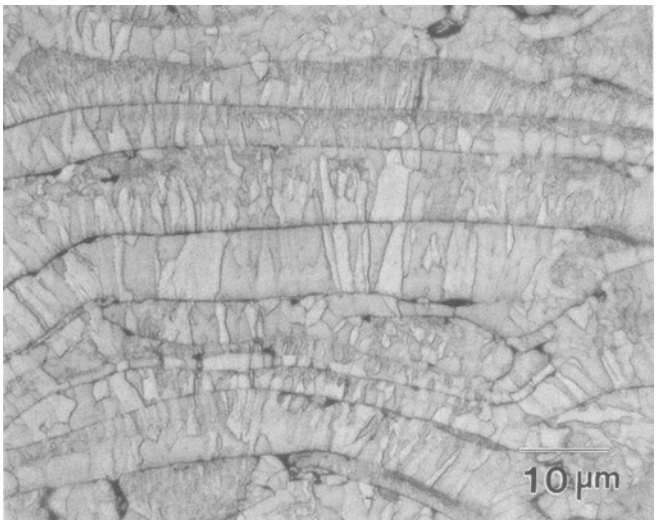

Fig. 7 Optical cross-sectional micrograph of an APS molybdenum deposit. Etchant: Murakami's reagent

posit could greatly reduce the heat transfer (Ref 40) and thereby reduce the cooling and solidification rates. The pervasive effect of this columnar microstructure is well illustrated in an APS molybdenum coating (Fig. 7), which displays columnar grain structures in most observable regions of the deposit.

Substrate surface morphology can greatly influence preferred orientation. This is depicted in Fig. 8, where the splat

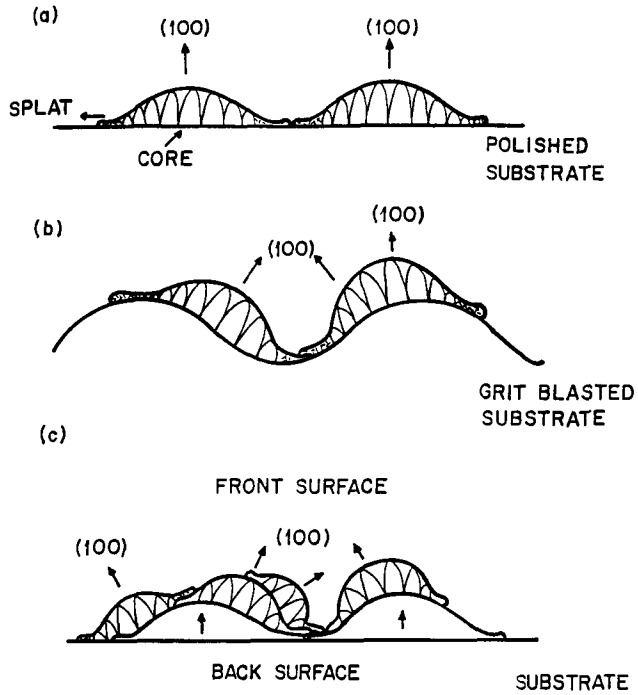

Fig. 8 Grain morphology and resulting texture in the plasma-sprayed splats

grain orientation on the roughened surface is compared to that for the smooth surface. Even in the case of the polished substrate

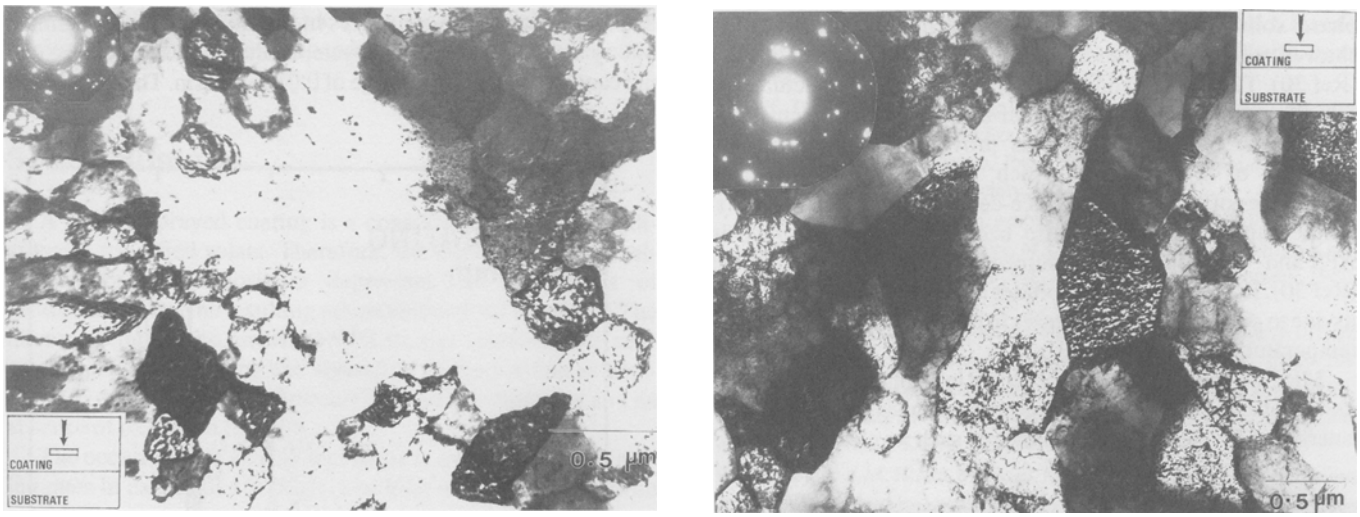

(a) (b)

Fig. 9 TEM micrographs from lateral section of a nickel deposit. (a) APS. (b) VPS

surface, the top layer of the coating shows no measurable texture (Table 6). This is because the accumulation of splats will likely result in roughening of the surface, effectively reducing measured texture (Fig. 8c).

In VPS, reverse-arc sputter cleaning provides an oxide-free surface, enabling high heat transfer to the substrate. The reduced oxidation of the particles for VPS also enhances better contact between splats and thus better heat conduction. Although the crystal growth morphology in VPS is similar to APS, the self-annealing process due to the high temperatures can cause recovery (stress relief) and recrystallization and can thus reduce or eliminate the preferred orientation.

Table 6 Texture measurements (I<200>/I<III>)(a)

Material	Process	Substrate condition	Intensity ratio, % Back side	Front side
Nickel	APS	Grit blasted	56	45
		Polished	96	48
	VPS	Grit blasted	(b)	49
		Polished	72	45
Ni-5Al	APS	Grit blasted	51	46
		Polished	65	43
	VPS	Grit blasted	(b)	43
		Polished	58	41

(a) Powder data file I<200>/I<III> = 42%. (b) Deposit could not be detached from substrate

4.3 *Grain Structure and Morphology*

Figure 9 shows TEM patterns of lateral sections (normal to surface) of the coating interior. Figure 9(a) is a micrograph of an APS nickel deposit. The microstructure agrees well with the cross-sectional images of Fig. 6(a) in terms of grain size and morphology. Mostly fine-grained regions are observed, with some large sections having similar orientations. The grain sizes are in the range of 0.1 to 0.3 μm. The TEM of the VPS deposit (Fig. 9b) shows a similar microstructure, with grain sizes in the range of 0.4 to 0.6 μm. Polygonized cells are also observed within the grains shown in Fig. 9(b), indicating incomplete recrystallization.

The boundaries between splats are distinct in the APS coating, as seen in Fig. 7, suggesting that splat individuality is maintained. This is depicted in the optical micrograph of the coating cross section (Fig. 10a). The distinctions between the splat layers are clearly defined. Oxide stringers separate these splat lamellae. A variety of microstructures are observed in the APS deposit, resulting from variations in particle trajectories, oxidation behavior, and melting efficiency. In VPS coatings, such distinct boundaries are not observed (Fig. 10b). Interdiffusion and recrystallization processes occur within the VPS coating due to the high temperatures and the absence of oxide layers, and a uniform and homogeneous deposit is obtained—implying superior physical and mechanical properties (Ref 11).

4.4 *Phase Formation*

The above model for microstructure development during plasma spray deposition suggests heterogeneous nucleation of the solid phase at the substrate, followed by planar growth of the interface. The large interfacial velocities suggest massive or partitionless solidification via supercooling. This is expected to result in considerable solute trapping and formation of metastable phases (Ref 41). Massive crystallization with heterogeneous nucleation frequently leads to columnar grain structures during rapid solidification (Ref 45). This effect of rapid solidification has been well illustrated in a plasma-sprayed deposit and has led to the formation of various metastable phases in the deposit associated with large undercooling and massive solidification effects.

In order to further examine the massive solidification effects of plasma spray deposition, a Ni-50Cr two-phase eutectic alloy was studied. The feedstock powder shows a two-phase eutectic structure consisting of nickel solid solution and β-chromium phase (Fig. 11). The APS coating shows a supersaturated single-

phase solid solution. Examination of the coating by TEM showed regions of spinodal decomposition within the coating (Ref 30). The VPS coating exhibited a two-phase structure, but this effect may be attributed to self-annealing subsequent to solidification. Evidence of this is provided by the TEM micrograph of the coating, which illustrates fine dispersed precipitates of chromium in a face-centered cubic nickel matrix. Solute supersaturation has also been commonly observed in APS and VPS coatings of a number of multicomponent alloys (Ref 30). In many cases precipitates are observed in VPS deposits due to self-annealing processes in the deposit during the high-temperature exposure.

Microcrystalline grains are observed in all of the sprayed deposits described here. Grain size shows a dependence on material characteristics. Single-component systems, such as elemental nickel and aluminum, show grain sizes in the range of 0.2 to 1.0 μm. In binary and multicomponent systems, the grain sizes can be significantly smaller, in the range of 0.05 to 0.1 μm. The VPS grains

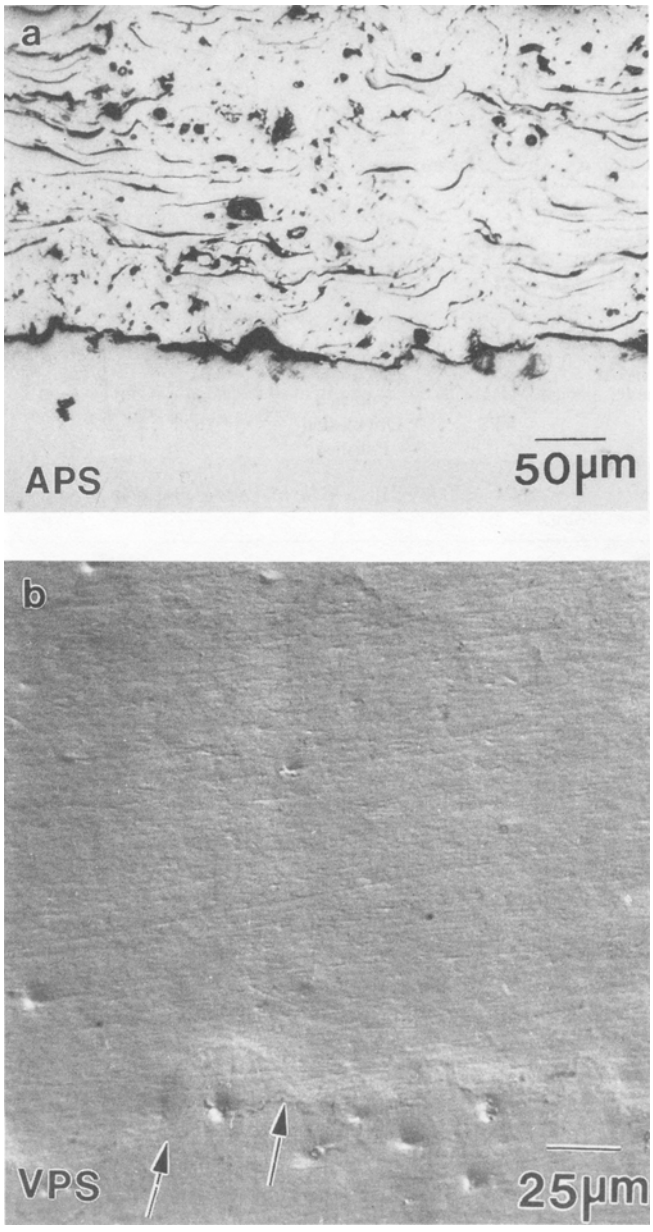

Fig. 10 Optical cross-sectional micrographs of a nickel deposit. (a) APS. (b) VPS. Arrows indicate the substrate/deposit interface

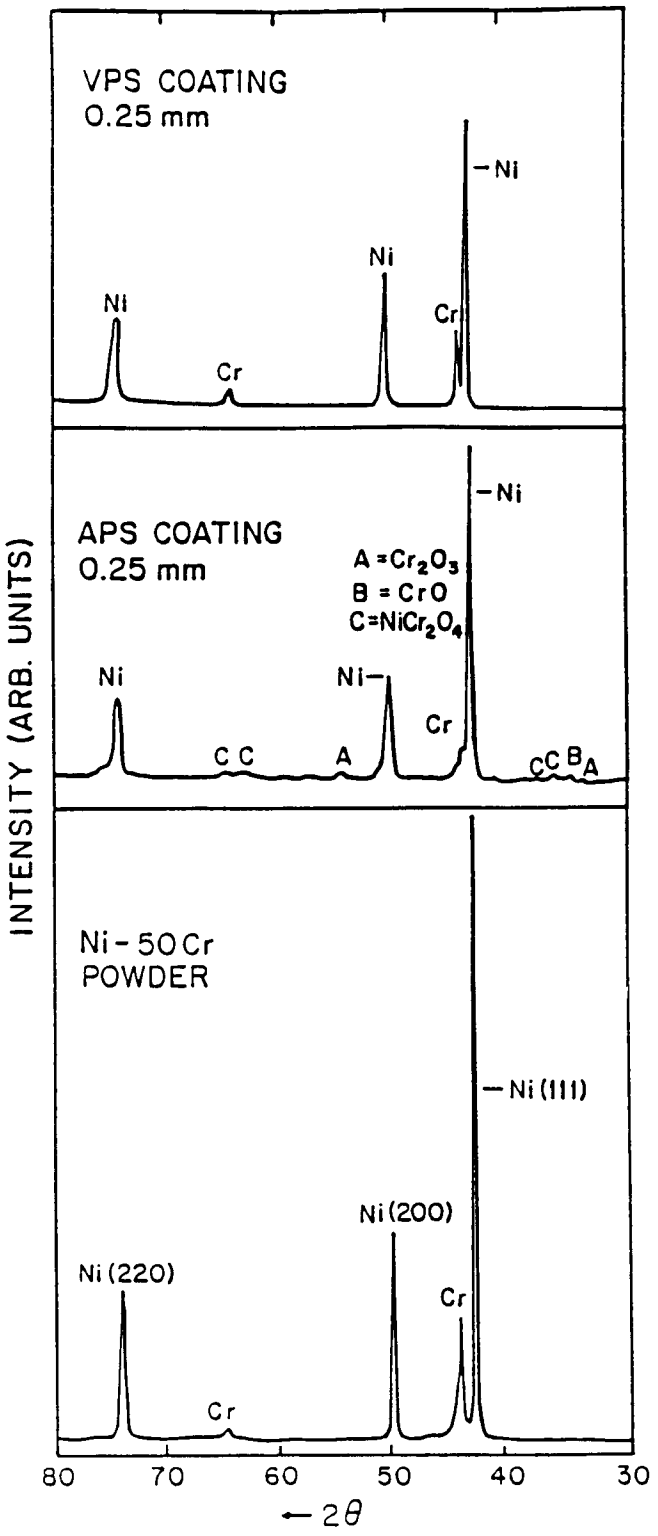

Fig. 11 X-ray diffraction patterns from a eutectic Ni-50Cr powder and APS and VPS deposits. Note the complete supersaturation of chromium in nickel in the APS deposit

are stress relieved and in some cases recrystallized. The morphology of grains varies, depending on the region within the splat.

5. Conclusions

A plasma-sprayed coating is a consolidation of many individually solidified splats. Therefore, the microstructure development of the deposit is dependent on the details of solidification and the resulting microstructures of the splats. The microstructure of the rim of the VPS-formed splat of nickel suggests a greater flattening and spreading of the particle as compared to APS. This arises from higher particle velocities and an absence of oxidation for VPS.

The occurrence of an RSP technique is confirmed, with cooling rates in excess of 10^6 deg/s, resulting in solidification front velocities greater than 10 cm/s with interface-controlled heat transfer. This results in the solidification front being morphologically stable, leading to columnar, partitionless solidification. In addition, at such interface velocities, a preferred <100> direction of crystal growth is expected to prevail in cubic metals. This is exhibited by a strong <100> texture on the back sides of nickel and nickel-aluminum coatings sprayed onto polished substrates.

The core region of the splat shows what is essentially a columnar microstructure, with a <100> direction normal to the columns. This is obtained by heterogeneous nucleation at the interface followed by columnar growth along <100> perpendicular to the interface. Each individual splat is textured, but a mutual misorientation develops as the deposit builds up. This is attributed to surface roughness created by grit blasting and nonuniform layering of splats. Reduction in texture can also occur due to a substantial reduction in cooling rates. In APS, this can occur in the presence of oxide layers, which limit effective heat transfer. In VPS, recrystallization can reduce or eliminate texture.

This study, although principally conducted for plasma spraying, has relevance to other thermal spray methods. The attributes of impact, spreading, and rapid solidification are common to all processes, and the deposit formation dynamics and ensuing microstructure development are similar.

Acknowledgments

The authors wish to thank G.A. Bancke for his invaluable assistance during plasma spraying and Dr. Rich Neiser for comments throughout the course of the study. This work was supported in part by the National Science Foundation DDM 9215846.

References

1. S. Sampath and H. Herman, Plasma Spray Forming Metals, Intermetallics and Ceramics, *J. Met.*, Vol 45 (No. 7), 1993, p 42-49
2. S. Safai and H. Herman, Plasma Sprayed Materials, *Treat. Mater. Sci. Technol.*, Vol 20, 1981, p 183-214
3. M. Moss, Dispersion Hardening in Al-V by Plasma Jet Spray Quenching, *Acta Metall.*, Vol 16, 1968, p 321-326
4. K.D. Krishnananda and R.W. Cahn, Properties of Plasma Sprayed Aluminum-Copper Alloys, *Proc. 2nd Int. Conf. Rapid Quenching*, Section I, B.C. Giessen and N.J. Grant, Ed., 1976, p 67-75
5. B.C. Giessen, M.N. Madhava, R.J. Murphy, R. Ray, and J. Surette, Sheet Production of an Amorphous Zr-Cu Alloy by Plasma Spray Quenching, *Metall. Trans. A*, Vol 8A, 1977, p 364-366
6. S.K. Das, E.M. Norin, and R.L. Bye, Ni-Mo-Cr-B Alloys: Corrosion Resistant Amorphous Hard Facing Coatings, Rapidly Solidified Metastable Materials, *MRS Symp. Proc.*, Vol 28, B.H. Kear and M. Cohen, Ed., Materials Research Society, 1984, p 233-237
7. V. Panchanathan, C.L. Tsai, and S. Whang, Rapidly Solidified Amorphous and Crystalline Alloys, *MRS Symp. Proc.*, Vol 8, B.H. Kear, B.C. Giessen, and M. Cohen, Ed., Materials Research Society, 1982, p 137-141
8. S. Sampath, B. Katz, and H. Herman, Vacuum Plasma Sprayed Hard Coatings, *Mém. Étud. Sci. Rev. Métall.*, Vol 88, May 1991, p 289-294
9. B. Gudmundsson and B.E. Jacobson, Microstructure and Erosion Resistance of Vacuum Plasma Sprayed CoNiCrAlY/Al_2O_3 Composite Coatings, *Mat. Sci. Eng.*, Vol A108, 1989, p 87-95
10. H. Takigawa, M. Hirata, M. Koga, M. Itoh, and K. Takeda, Applications of Hard Coatings by Low Pressure Plasma Spray, *Surf. Coat. Technol.*, Vol 39/40, 1989, p 127-134
11. S. Sampath and H. Herman, Microstructures of Vacuum Plasma Sprayed Coatings, *Thermal Spray: Advances in Coating Technology*, D.L. Houck, Ed., ASM International, 1988, p 1-7
12. S. Sampath, B. Gudmundsson, R. Tiwari, and H. Herman, Plasma Spray Consolidation of Ni-Al Intermetallics, *Thermal Spray Research and Applications*, T. Bernecki, Ed., ASM International, 1990, p 357-362
13. R. Tiwari, S. Sampath, and H. Herman, Plasma Spray Consolidation of High Temperature Composites, *Mat. Sci. Eng.*, Vol A144, 1991, p 127-131
14. M.R. Jackson, J.R. Rairden, J.S. Smith, and R.W. Smith, Production of Metallurgical Structures by Rapid Solidification Plasma Deposition, *J. Met.*, Vol 33 (No. 11), 1981, p 23-27
15. R.W. Smith, D.V. Rigney, J.S. Smith, and J.R. Rairden, Plasma Deposition Effects on Structures and Properties of RSPD Alloys, *Rapid Solidification Processing: Principles and Technologies*, Vol III, R. Mehrabian, Ed., National Bureau of Standards, 1982, p 468-473
16. A.M. Johnson, J.S. Kelm, R.W. Smashey, D.V. Rigney, and T.G. Wakeman, Aircraft Engine Gas Turbine Component Fabrication Concepts using RSPD, *Rapid Solidification Processing: Principles and Technologies*, Vol III, R. Mehrabian, Ed., National Bureau of Standards, 1982, p 650-661
17. T.L. Cheeks, M.E. Glicksman, M.R. Jackson, and E.L. Hall, Temperature Effects on Plasma Deposition of Ni-base Materials, *Rapid Solidification Processing: Principles and Technologies*, Vol III, R. Mehrabian, Ed., 1982, p 118-123
18. A.M. Ritter and M.R. Jackson, Microstructural Characterization of RSPD Structures, *Rapid Solidification Processing: Principles and Technologies*, Vol III, R. Mehrabian, Ed., National Bureau of Standards, 1982, p 118
19. E. Pfender, Fundamental Studies Associated with the Plasma Spray Process, *Surf. Coat. Technol.*, Vol 34, 1988, p 1-14
20. A. Vardelle, M. Vardelle, R. McPherson, and P. Fauchais, Study of the Influence of Particle Temperature and Velocity Distribution within a Plasma Jet Coating Formation, *Proc. 9th Int. Thermal Spray Conf.*, The Hague, Netherlands, 1980, p 155-161
21. J.M. Houben, "Relationship of the Adhesion of Plasma Sprayed Coatings to the Process Parameters: Size, Velocity and Heat Content of the Spray Particles," Ph.D. thesis, Technische Universiteit Eindhoven, Eindhoven, Netherlands, Dec 1988
22. R.C. Dykhuizen, Review of Impact and Solidification of Molten Thermal Spray Droplets, *J. Therm. Spray Technol.*, Vol 3 (No. 4), 1994, p 351-361
23. M. Vardelle, A. Vardelle, A.C. Leger, P. Fauchais, and D. Gobin, Influence of Particle Parameters at Impact on Splat Formation and Solidifi-

cation in Plasma Spraying Process, *J. Therm. Spray Technol.*, Vol 4 (No. 1), 1994, p 50-58

24. C. Moreau, P. Gougeon, and M. Lamontagne, Influence of Substrate Preparation on the Flattening and Cooling of Plasma Sprayed Particles, *J. Therm. Spray Technol.*, Vol 4 (No. 1), 1994, p 25-33
25. H. Herman, Plasma Sprayed Coatings, *Sci. Am.*, Vol 256 (No. 9), Sept 1988, p 112-115
26. V. Wilms, Ph.D. thesis, State University of New York, Stony Brook, NY, 1978
27. C. Moreau, P. Cielo, M Lamontagne, S. Dallaire, J.C. Krapez, and M. Vardelle, Temperature Evolution of Plasma Sprayed Niobium Particles Impacting on a Substrate, *Surf. Coat. Technol.*, Vol 46, 1991, p 173-187
28. C. Moreau, P. Cielo, and M. Lamontagne, Influence of Coating Thickness on the Cooling Rates of Plasma Sprayed Particles Impinging on a Substrate, *Surf. Coat. Technol.*, Vol 53, 1992, p 107-114
29. P. Duwez, Structure and Properties of Alloys Rapidly Quenched from the Liquid State, *Trans. ASM*, Vol 60, 1967, p 607-633
30. S. Sampath, "Rapid Solidification during Plasma Spraying," Ph.D. thesis, State University of New York, Stony Brook, NY, 1989
31. M. Cohen, B.H. Kear, and R. Mehrabian, Rapid Solidification Processing—An Outlook, *Rapid Solidification Processing: Principles and Technologies*, Vol III, R. Mehrabian, B.H. Kear, and M. Cohen, Ed., Claitors, 1980, p 1-23
32. H. Matyja, B.C. Giessen, and N.J. Grant, The Effect of Cooling Rate on the Dendrite Arm Spacing of Splat Cooled Aluminum Alloys, *J. Inst. Met.*, Vol 96, 1968, p 30-32
33. H. Jones, Experimental Methods in Rapid Quenching From the Melt, *Treat. Mater. Sci. Technol.*, Vol 20, 1981, p 26-71
34. K. Murakami, T. Okamoto, Y. Miyamoto, and S. Nakazono, Rapid Solidification and Self-Annealing of Fe-C-Si Alloys by Low Pressure Plasma Spraying, *Mat. Sci. Eng.*, Vol A117, 1989, p 207-214
35. R.C. Ruhl, Cooling Rates in Splat Cooling, *Mat. Sci. Eng.*, Vol 1, 1968, p 313-320
36. S.C. Huang, R.P. Laforce, A.M. Ritter, and R.P. Goehner, Rapid Solidification Characteristics in Melt Spinning a Ni-base Superalloy, *Metall. Trans. A*, Vol 16A, 1985, p 1773
37. P. Predecki, A.W. Mullendore, and N.J. Grant, A Study of Splat Cooling Technique, *Trans. Metall. Soc. AIME*, Vol 233, 1965, p 1581-1586
38. D R. Harbur, J.W. Anderson, and W.J. Maramen, Rapid Quenching Drop Smasher, *Trans. Metall. Soc. AIME*, Vol 233, 1965, p 1581-1586
39. T.R. Anantharaman and C. Surayanarayana, Rapidly Solidified Metals, *Key Eng. Mater.*, Vol 17, 1987, p 80-86
40. P.H. Shingu and R Ozaki, Solidification Rate in Rapid Conduction Cooling, *Metall. Trans. A*, Vol 6A, 1975, p 33-37
41. M. Cohen and R. Mehrabian, Some Fundamental Aspects of Rapid Solidification, *Rapid Solidification Processing: Principles and Technologies*, Vol III, R. Mehrabian, Ed., National Bureau of Standards, 1980, p 1-26
42. S. Safai and H. Herman, Microstructural Investigation of Plasma Sprayed Al-Coatings, *Thin Solid Films*, Vol 45, 1977, p 295-307
43. R.W. Cahn, *Recrystallization, Grain Growth and Textures*, American Society for Metals, 1966, p 99-100
44. C.S. Barret and T.B. Massalski, *Structure of Metals*, 3rd ed , Pergamon Press, 1980
45. E. Hornbergen, Phase-Structure and Micro-Structure in Rapidly Quenched Alloys, *Rapidly Quenched Metals*, S. Steeb and H. Warlimont, Ed., Elsevier, 1985, p 785-796